The Aeronautical Journal (2024), **128**, pp. 2530–2544
doi:10.1017/aer.2024.88

RESEARCH ARTICLE

Numerical simulation of different aircraft sub-floor structures during ditching

B. Wang[1,2], L. Nie[3] and Y. Ren[1,2]

[1]College of Mechanical and Vehicle Engineering, Hunan University, Changsha, Hunan 410082, China
[2]State Key Laboratory of Advanced Design and Manufacturing for Vehicle Body, Hunan University, Changsha, Hunan 410082, China
[3]China Academy of Aerospace Science and Innovation, Beijing, 100086, China
Corresponding author: Y. Ren; Email: renyiru@hnu.edu.cn

Received: 19 April 2024; **Revised:** 28 May 2024; **Accepted:** 10 June 2024

Keywords: ditching; aircraft skin; crashworthiness; smoothed particle hydrodynamics

Abstract

To enhance the impact resistance capacity and ensure the floatability of aircraft after ditching, the slamming response of three types of aircraft sub-floor structures are investigated including the flat, cylindrical and ellipsoidal under floor. A coupled Finite Element-Smooth Particle Hydrodynamic (FE-SPH) method is employed with focus on non-linear structural collapse in fluid-structure interaction. The material is defined by bilinear elastic plastic law, and the strain rate effect is taken into account. Further, comparison and analyses are performed in terms of acceleration, local pressure and strains at different speeds. Results show that conventional flat sub floor structures perform poorly during ditching due to excessive peak acceleration and pressure. By contrast, the peak acceleration of ellipsoidal under floor is lower at all measured speeds and the pressure on the sides is reduced. Moreover, the ellipsoidal sub-floor with bi-directional curvature generates smaller plastic strain and deflection of skin, demonstrating better mechanical properties in water impact scenarios.

Nomenclature

FE	finite element
SPH	smooth particle hydrodynamic
CFC	SAE channel filter class
EOS	equation of state
ACC	accelerometer
P	pressure transducer
E_i	linear in internal energy
C_i	material constant
r	position
m	mass
p	pressure
v	velocity
ρ	density
μ	volumetric strain

1.0 Introduction

Ditching is the emergency procedure for landing aircraft on water, which must be taken into account by the aircraft manufacturers of all countries in the certification process. The ditching process of an aircraft can be divided into four stages: approach, impact, landing, and floatation [1, 2]. The impact

© The Author(s), 2024. Published by Cambridge University Press on behalf of Royal Aeronautical Society.

https://doi.org/10.1017/aer.2024.88 Published online by Cambridge University Press

stage is crucial for the success of ditching. During the impact stage, the aircraft is subjected to extreme overloads. There is a huge impact on the fuselage belly, which leads to structural deformation or damage. Moreover, excessive deformation and rupture of the fuselage will affect the floatability of the aircraft and the safe egressing of passengers.

The issue of structures impacting water surfaces is first addressed by Karman, who developed the physical concept of the problem in 1929 [3]. Some researchers conducted extensive theoretical studies on the vertical water entry problem for two-dimensional objects. With zero gravity and a constant entry velocity, significant progress is made with both linear theories and the theories of treating the free surface conditions exactly [4, 5]. Researchers agree that the impact processes involved in a fluid-structure interaction are extremely complex, with the influence of water kinetics and the underlying physics still not properly understood [6, 7]. Furthermore, for the complex aircraft structure, the theoretical research is difficult to analyse in a comprehensive and in-depth manner [8]. Hughes conducted experimental studies on the impact resistance of metal helicopter under floor structures when hitting the water [9]. Furthermore, he discussed the recommendations for design changes that could improve the level of crashworthiness and summarised the advancements and achievements in the experimental aspects of aircraft water impact resistance since the 1980s [10]. In order to get a more realistic data of the aircraft impact water, a full-scale WG30 helicopter test is performed, and discussed challenges in predicting measured acceleration and pressure peaks using numerical modelling methods [11]. The crucial vertical drop tests were conducted comparing rigid surfaces and water surfaces, providing valuable reference data for analysing such problems [12, 13]. These research studies identified the classification of failure and damage on soft and hard surfaces, providing a framework and catalyst for the development of numerical methods.

With advancements in computing power and simulation tools, numerical modeling techniques have provided satisfactory solutions for predicting the nonlinear hydrodynamic response of aircraft during ditching [14–17]. Smoothed particle hydrodynamics, as a numerical method, can easily handle distortions and complex boundaries, and its stable results make it widely applicable to large-scale fluid-structure coupling simulations [18–20]. From 2000 to 2003, the CAST project, Crashworthiness of Helicopter on Water: Design of Structures using Advanced Simulation Tools, examined various techniques for simulating helicopter ditching, including the application of SPH [21, 22]. This research is extended through the GARTEUR HC/AG-15 project [23], focusing on enhancing SPH methods for helicopter ditching applications [24]. The subsequent program, Smart Aircraft in Emergency Situations (SMAES), continued this investigation from 2011 to 2014 [25]. Woodgate quantified the impact of numerical parameters in SPH, including the boundary conditions between water and solid, as well as the influence of the number and type of smoothed particles for ditching [26]. Furthermore, a weakly compressible SPH method is developed to investigate the hydrodynamic and dynamic behaviour of a helicopter ditching [27]. The simulation model is established for an AW159 helicopter ditching based on SPH method, the cases of a vertical drop of the helicopter at no sea-state and on the crew of a wave were simulated [28]. These studies used numerical simulation methods to investigate landing angle problems and sea state problems during ditching. However, the problem of entering water with multiple shapes has been confined to the investigations of two-dimensional objects. Currently, there have been limited studies of different shapes of three-dimensional aircraft sub-floor during ditching.

The present work addresses the water slamming response of three types of sub-floor structure using the FE-SPH method, organised as follows. In Section 2, the principles of the SPH method are briefly described and the loads of an aircraft landing versus water landing are analysed. In Section 3, the accuracy of the numerical method is verified by vertical water impact experiments of a semi-cylindrical steel structure conducted in the Italian Laboratory for Impact Tests on Aerospace Structures (LISA). The acceleration values and three pressure values at a variety of speeds are compared separately. Furthermore, the structural deformation of the steel skin is evaluated. In Section 4, three shapes of sub-floor structures are built, including a flat without curvature, a cylindrical surface with single curvature and an ellipsoidal surface with double curvature. Several parameters are compared to analyze the loading of the three structures at different speeds during impacting water, including acceleration,

https://doi.org/10.1017/aer.2024.88 Published online by Cambridge University Press

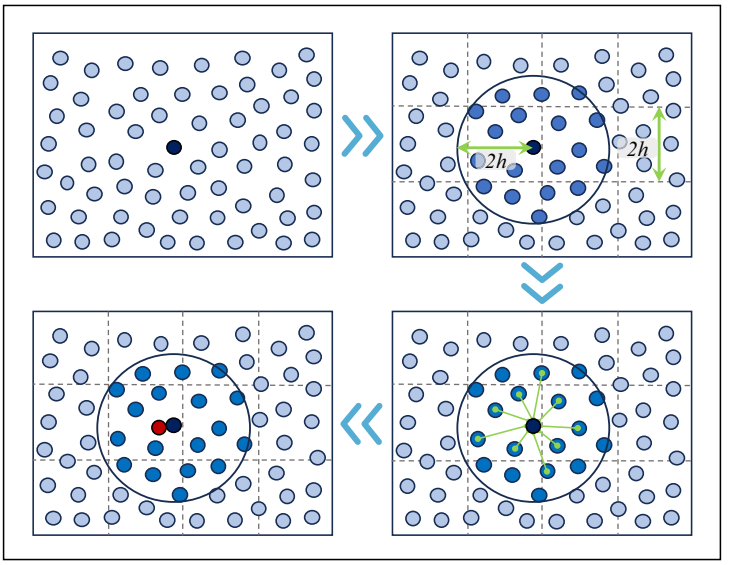


Figure 1. *Brief overview of SPH method.*

local pressure, skin deflection and plastic strain. The better shape of the sub-floor structure for aircraft is investigated by assessing the effects of curvature of the sub-floor shape during ditching.

2.0 Numerical model

SPH is a mesh-free method originally proposed by Lucy, Gingold, and Monaghan in 1977 [29, 30]. It accurately and stably solves a set of partial differential equations without the need for any grid connecting the particles. The SPH method employs a discrete set of smooth particles with position, velocity and mass attributes to approximate the values and derivatives of continuous variables. Subsequently, it calculates the weighted averages of all neighbouring particles. A simplified overview of the SPH method is depicted in Fig. 1. In SPH, fluid is treated as a collection of particles, each possessing associated physical properties such as position $r(t)$, mass $m(t)$, density $\rho(t)$, pressure $p(t)$, and velocity $v(t)$. The computational domain is then discretised into spatial bins of size 2 h, and particles within the particle's own space and adjacent spaces are identified. For a given particle, only interactions with neighbouring particles within a distance less than 2 h are considered. The interactions are computed for the given particle and the selected neighbouring particles by solving the following NS equations:

$$\frac{dv_i}{dt} = -\sum_j m_j \left(\frac{p_i}{\rho_i^2} + \frac{p_j}{\rho_j^2} + \prod_{ij} \right) \nabla_i W_{ij} + F_i, \tag{1}$$

$$\frac{d\rho_i}{dt} = \sum_j m_j \left(v_i - v_j \right) \nabla_i W_{ij}. \tag{2}$$

The position and velocity of the particle for the next time step are then updated based on the results of the following calculation. Figure 2 illustrates the detailed calculation cycle.

$$r_i(t + \Delta t) = r_i(t) + \Delta t v_i(t)\,, \tag{3}$$

$$v_i(t + \Delta t) = v_i(t) + \Delta t a_i(t)\,. \tag{4}$$

https://doi.org/10.1017/aer.2024.88 Published online by Cambridge University Press

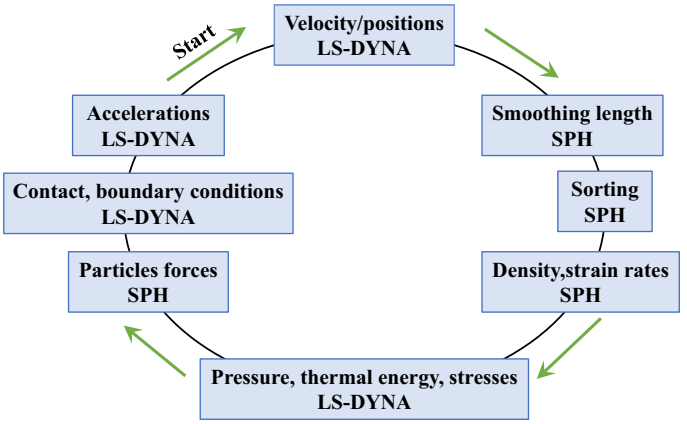


Figure 2. *The calculation cycle of SPH method.*

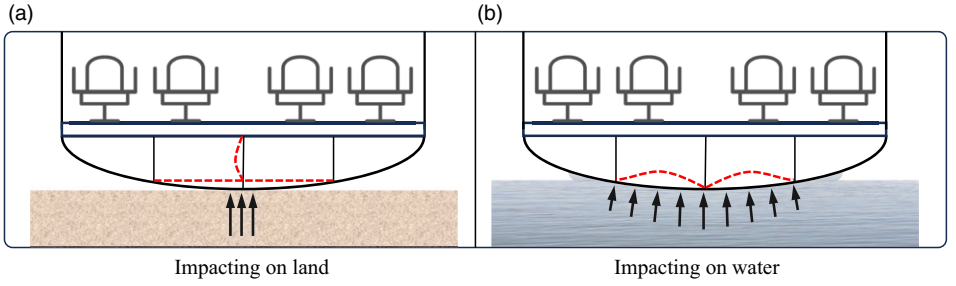


Figure 3. *Comparison between impact on a rigid floor and on water.*

It is widely recognised that structural loading for water impact is significantly different to hard surfaces [31]. As shown in Fig. 3, the aircraft's kinetic energy is absorbed by the plastic deformation of the metal structure during impact on a hard surface, reducing the impact load and acceleration to survivable levels. However, in the case of water impact, the landing gear and conventional flat under floor structures perform poorly in absorbing impact energy [32, 33]. The impact load is distributed along the skin, and energy absorption depends primarily on bending behaviour of the skin as well as the limited plastic collapse of supporting frames [34, 35]. In severe cases, aircraft skin rupture or inability to transmit impact loads could significantly reduce the efficiency of sub-floor structural energy absorption. Internal structures may also suffer secondary damage due to water ingress [36]. Therefore, it is imperative to investigate the effects of water impact on different structures to enhance the survivability of passengers during aircraft emergency water landing.

Numerous accident cases have demonstrated that the aircraft skin rupture during ditching is the main reason affecting passenger survival rates [37, 38]. To investigate the aircraft under floors impacting water surfaces and analyse the load on aircraft skin during water impact, the Italian Center of Aerospace Research (CIRA) conducted a water entry impact experiment at the Laboratory for Impact Tests on Aerospace Structures [39]. The test specimen of steel structure is dropped into the water at different velocities to generate an experimental database for validating numerical models. The test specimen is a semi-cylindrical aircraft skin reinforced with three frames positioned symmetrically on both sides and at the centre of the skin. To secure the structure on the drop tower trolley, L-shaped and U-shaped steels are mounted above the structure. Both the skin and frames are constructed using 2 mm thick hot-rolled steel (DD11). The material is defined by bilinear elastic plastic law and takes into account the strain rate

https://doi.org/10.1017/aer.2024.88 Published online by Cambridge University Press

effect by adding the stress-plastic strain curve. As the experimental impact velocities are not sufficient to cause damage to the material, the material model does not need to consider material failure. The structure had a length of 1,200 mm, a cross-sectional radius of 475 mm, a central circular hole with a diameter of 150 mm in the frames, a specimen weight of 66.4 kg and the trolley weight of 174 kg.

The structural model employed shell elements with a total of 7,592 elements. All shell elements are implemented in the Belytschko-Tsay format, and the selected thicknesses are consistent with the experimental setup. As there is no structural failure observed in the experiments, interconnection between models is established through merged nodes. The material model for the drop tower trolley utilised the rigid model, with the addition of mass points at the centre to simulate the actual trolley weight. To align with experimental constraints, only the vertical degrees of freedom for the trolley are retained.

The water model is structured using the SPH algorithm. The water domain consists of a cubic shape measuring 2,000 mm × 1,600 mm × 800 mm, composed of 40,000 particles. The Particle Approximation Theory employs an enhanced fluid formulation. The equation of state (EOS) is linear in internal energy (E_i) and it defines the pressure-volume relationship as:

$$\rho = C_0 + C_1\mu + C_2\mu^2 + C_3\mu^3 + \left(C_4 + C_5\mu^2 + C_6\mu^3\right)E_i, \tag{5}$$

where in this case μ is the volumetric strain defined as:

$$\mu = \frac{\rho}{\rho_0} - 1, \tag{6}$$

ρ is the current density, ρ_0 is the reference water density and $C_i(i = 1, 2, \ldots, 6)$ are material constants. The following values are used: $C_1 = 2.723$ GPa, $C_2 = 7.727$ GPa, $C_3 = 14.66$ GPa, $C_0 = C_4 = C_5 = C_6 = 0$ [40].

The penalty methods are implemented with the contact interaction between the structural model and the water model, and the soft constraint mode is activated. The soft constraint option's force scaling factor is set to 0.5. In the soft constraint option, the interface stiffness is based on the nodal mass and the global time step size. This method of calculating interface stiffness will typically give a much higher stiffness value than would be obtained using the bulk modulus. Therefore, this method is the preferred approach when water interacts with metals. Moreover, self-contact is enabled for the skin to prevent penetration. The structural model is initialised with impact velocities identical to those in the experiments, and gravitational effects are taken into account. Acceleration data are collected at the top plate of the model, representing the average acceleration at various points on the plate. Pressure values obtained by dividing the collected force by the corresponding area. The experiments involve drop tests with velocities of 3 m/s, 8 m/s and 10 m/s, and the overall simulation model are depicted in Fig. 4.

3.0 Numerical simulation results

3.1 Skin deformation

To analyse the impact behaviours of the aircraft skin structure by simulation, the experimental and numerical results obtained from Borrelli and Grimaldi are used to validate the devised numerical model [41, 42]. The measured deformation sections are illustrated in Fig. 5. In Fig. 5(a), for an entry velocity of 8 m/s, the maximum relative displacement at Skin Section I is 31 mm. In Fig. 5(b), with an entry velocity of 10 m/s, the maximum relative displacement at Skin Section II is 45 mm. As shown in Fig. 5, there is a strong correlation between the experimental results and the present. Both values exhibit an error within 10% when compared to the experimental measurements obtained from the specimen post-impact. In the present results, the side of the skin is deformed outwards by the bending moment generated by the bottom deformation. This trend of the predicted displacements is closer to the experimental results and is not found in previous results. The symmetry of the deformation on both sides of the skin at different

https://doi.org/10.1017/aer.2024.88 Published online by Cambridge University Press

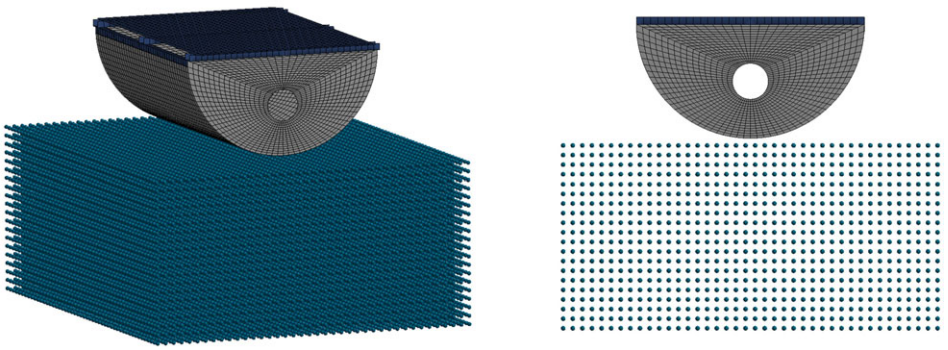


Figure 4. *Steel structure finite element model and water particle model.*

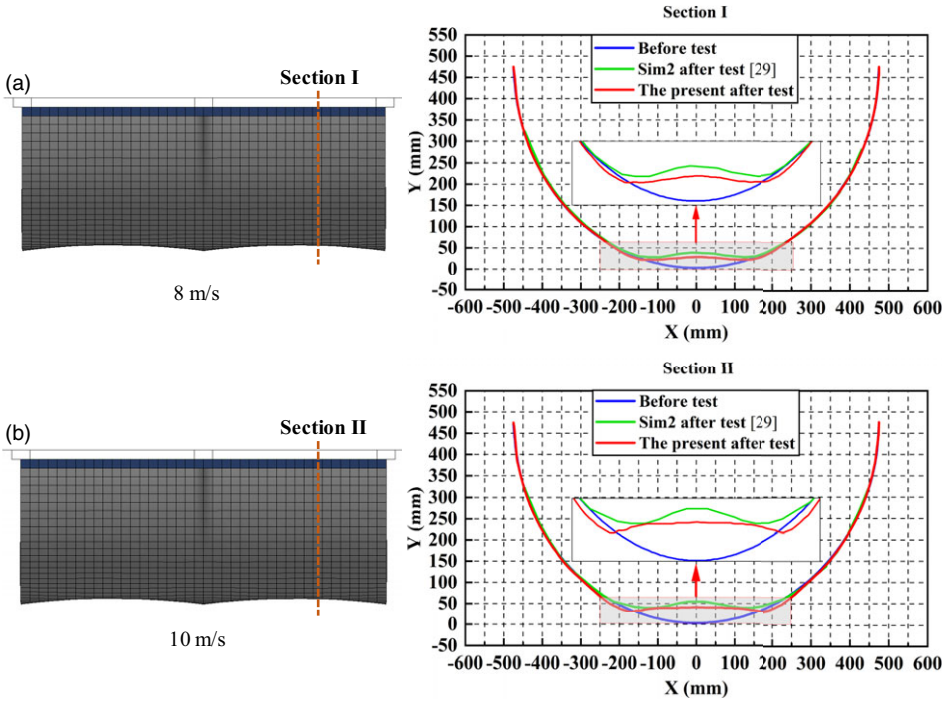


Figure 5. *Shape of the skin and measurement of deformation of section [42].*

velocities aligns closely with the experimental findings, providing further evidence of the accuracy of the simulations.

3.2 Acceleration and pressure

The positions for the accelerometer (ACC1, ACC2, ACC3 and ACC4) and pressure transducer (P1, P2, P4, P6 and P7) are illustrated in Fig. 6. Due to symmetry considerations, three locations on the skin are designated as pressure sensor locations in the simulation.

The acceleration-time histories and pressure-time histories at different velocities are depicted in Figs. 7, 8 and 9. Sim1 represents the simulation results from Borrelli, Sim2 from Grimaldi and Sim1 employs filtering with SAE Channel Filter Class (CFC) 60, and Sim2 uses CFC180 for filtering.

https://doi.org/10.1017/aer.2024.88 Published online by Cambridge University Press

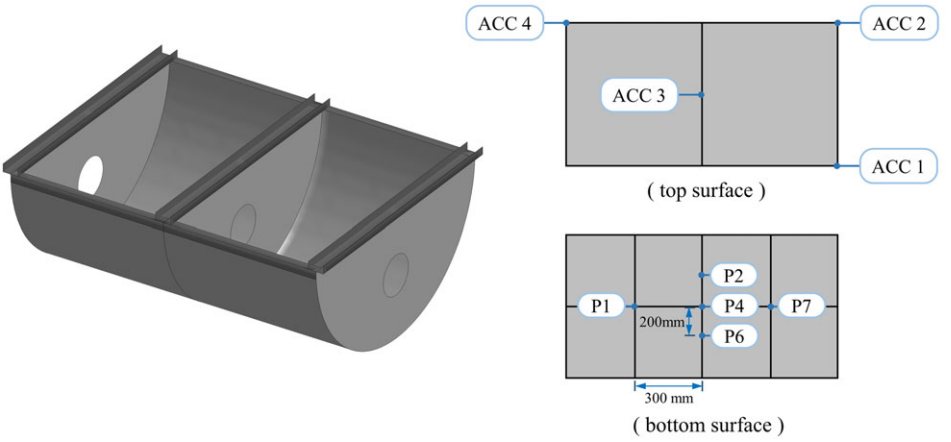


Figure 6. *Transducer deployment location [41].*

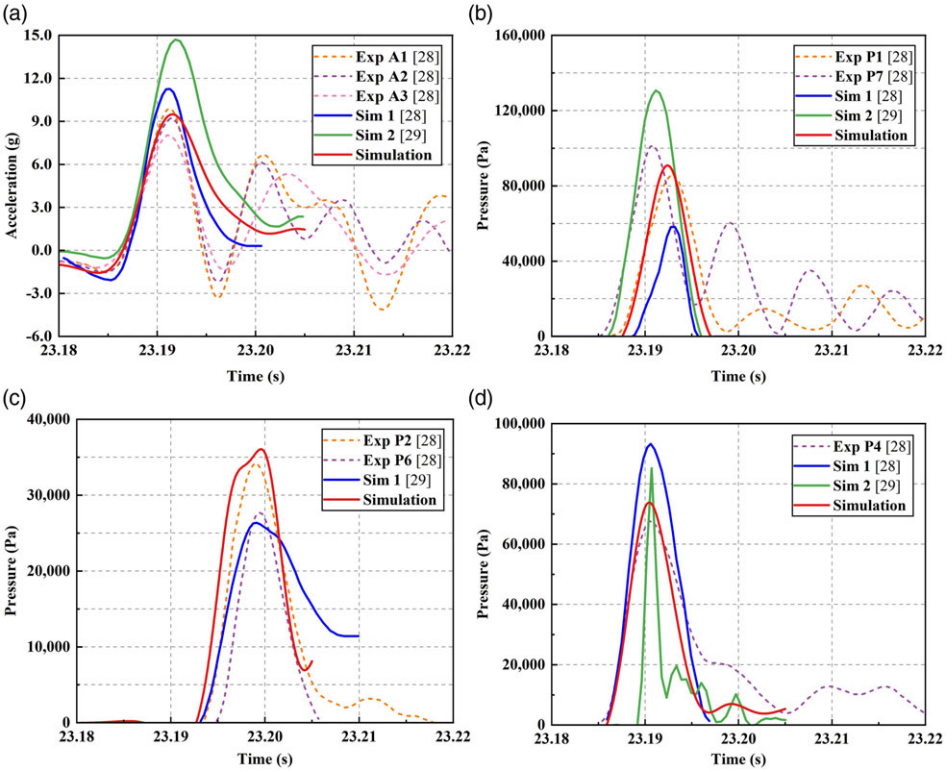


Figure 7. *At 3 m/s, time histories of acceleration and pressures [41, 42].*

The water model of Sim1 utilises a mixed SPH-FE approach and Sim2 used the SPH method to model. In present simulation, both experimental and simulated data are subjected to filtering with the SAE Channel Filter Class (CFC) 60 Hz [43]. In order to facilitate comparison, all the numerical curves are adjusted on the time scale to fit the experimental curves.

As depicted in Figs. 8(a) and 9(a), Sim1 and Sim2 demonstrate a strong correlation in peak accelerations at impact velocities of 8 m/s and 10 m/s. However, as depicted in Fig. 7(a), at an impact velocity

https://doi.org/10.1017/aer.2024.88 Published online by Cambridge University Press

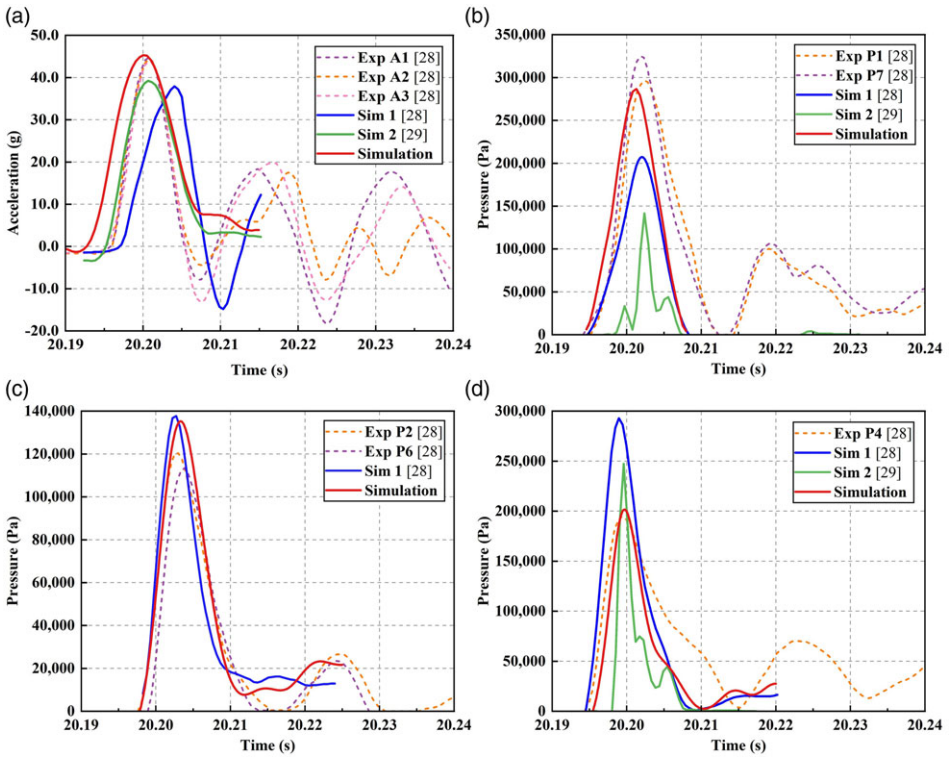


Figure 8. *At 8 m/s, time histories of acceleration and pressure [41, 42].*

of 3 m/s, the water models of Sim1 and Sim2 exhibit excessive rigidity resulting in an overestimation of the acceleration peak. The results show that the water model fails due to excessive rigidity when the impact velocity is insufficient to induce plastic deformation in the specimen. With regards to pressure, accurate predictions are observed in soft areas (bays), while overestimations are evident in stiff areas (under the frames).

Building upon the findings of previous research, this study further refined the model parameters. The entire water pool model is represented using a particle-based approach. The particle spacing of the present simulation is chosen taking into account calculation accuracy and computational cost. To enhance stability in contact calculations, merged node connections are established between various models. The soft constraint formulation is implemented, and the scale factor for constraint forces of the soft constraint option is set to 0.5. The correlation between numerical and experimental peak accelerations at different velocities is significantly improved, with errors kept within 5%. Pressure values is the most challenging to measure. Beneath the stiff areas, the optimisation of the parameters demonstrated noticeable improvement, with errors controlled within 10%. In the soft areas, the predicted values aligned closely with experimental results when no plastic deformation occurred in the material. While there are still some errors in the predicted values at the lateral positions beneath the stiff areas, notable progress is observed compared to previous results. All errors of simulation are within 20%, with six peak data errors below 5%, showcasing strong correlations. Particularly, peak accelerations exhibit excellent agreement with experimental values across different impact velocities.

4.0 Simulation of different sub-floor shapes

Three different shapes of helicopter sub-floor structures are established, as shown in Fig. 10. The sub-floor shapes include the flat, the cylindrical surface with transverse curvature and the ellipsoid with

https://doi.org/10.1017/aer.2024.88 Published online by Cambridge University Press

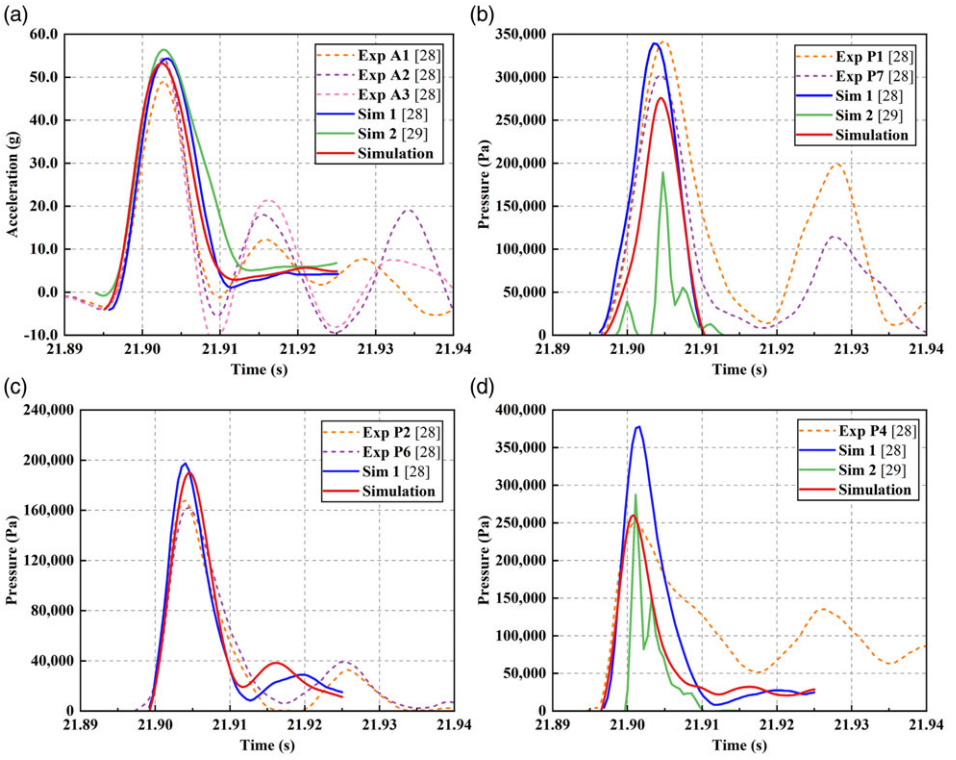


Figure 9. *At 10 m/s, time histories of acceleration and pressure [41, 42].*

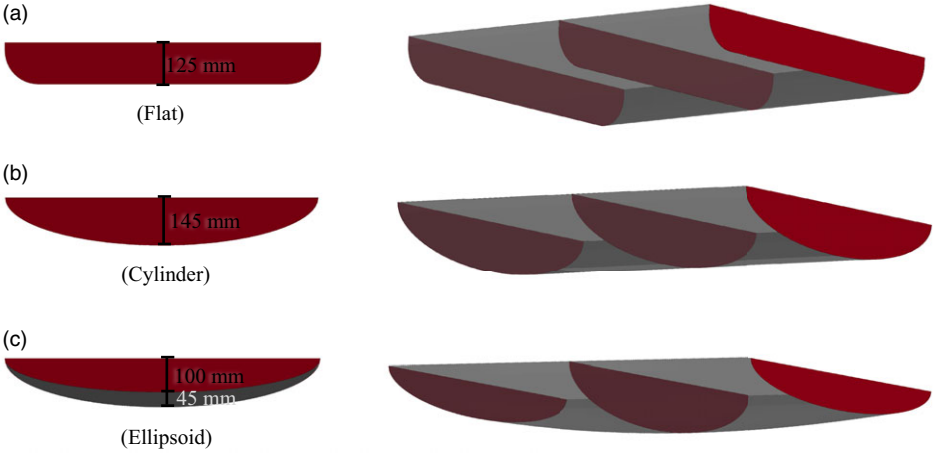


Figure 10. *Under floor models.*

double curvature. A coupled FE-SPH method is employed, which is not only capable of predicting non-linear structural collapse, but also represents the underlying kinematics of water and pressure transmissibility. As the weight of the floor structure is primarily concentrated on the trolley, weight variations among the models are less than 1% of the overall weight. Therefore, the impact of weight variation on the results can be disregarded. The impact velocities are 3 m/s, 8 m/s and 10 m/s, respectively.

https://doi.org/10.1017/aer.2024.88 Published online by Cambridge University Press

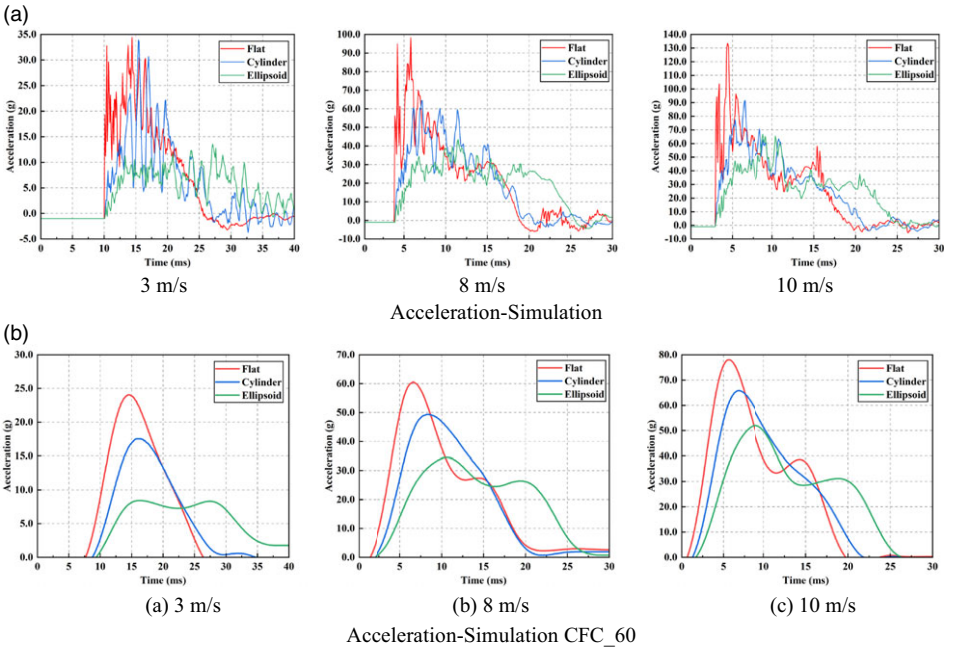


Figure 11. *Time history of acceleration.*

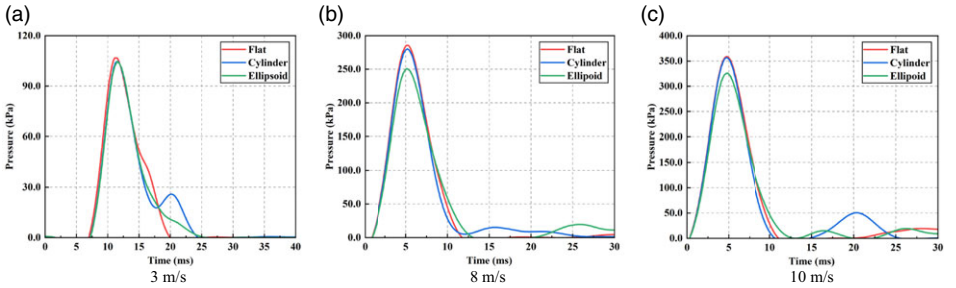


Figure 12. *Time history of pressure P4.*

Acceleration data are collected from the top plate, and the values represent the average acceleration at various points on the plate. As depicted in Fig. 11, the peak acceleration upon water impact exhibits a gradient distribution among the flat, cylinder and ellipsoid shapes. The flat surface experiences the highest impact acceleration, while the ellipsoid surface encounters the lowest. Experimental results demonstrate that appropriately shaped surfaces can effectively mitigate the impact during structural water entry. With increasing velocity, the deceleration effect persists, although its efficacy diminishes gradually. In short, at different speeds, the ellipsoid is the best of the three shapes.

The P4 pressure sensor is positioned at the central location of the under floor. And it is the initial contact point with water after the descent of all structures. The pressure-time history of P4 is illustrated in Fig. 12. As the structure enters the water at 3 m/s, the peak pressures at different locations on various under floor structures are nearly identical. With an increase in velocity, the pressure levels on the flat and cylinder surfaces remain consistent, while the advantage of the ellipsoid shape becomes apparent, displaying significantly lower pressures on its skin surface compared to the other two structures.

https://doi.org/10.1017/aer.2024.88 Published online by Cambridge University Press

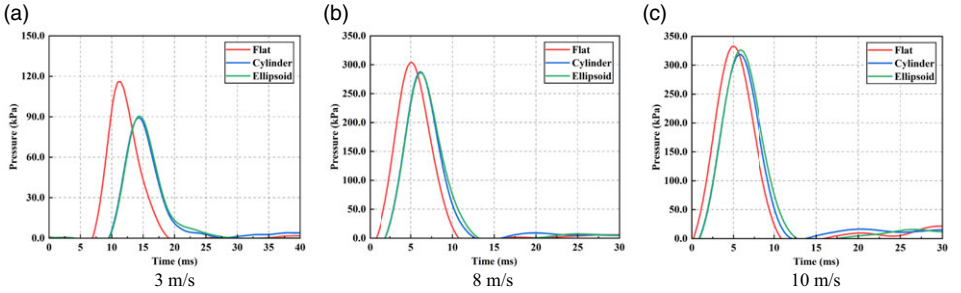


Figure 13. *Time history of pressure P1.*

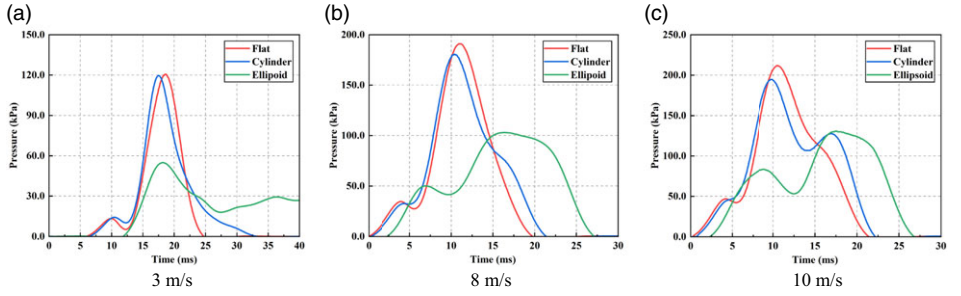


Figure 14. *Time history of pressure P2.*

The pressure-time curve for P1 is depicted in Fig. 13. As the structure enters the water at 3 m/s, the pressure at P1 on the flat surface is significantly higher than on the curved surface. With an increase in velocity, the difference between the two gradually diminishes. The pressures at P1 for the cylinder and ellipsoid surfaces are nearly identical, and at a velocity of 10 m/s, the slightly smaller peak pressure on the ellipsoidal surface compared to the cylinder.

From Fig. 14, it can be observed that, due to the curvature of the ellipsoid surface deflecting the water flow radially, the surface deformation changes relatively little, thereby minimising the loads at these locations. At 3 m/s, the pressure at P2 on the ellipsoid surface is comparable to that on the flat surface, as the curvature of the ellipsoidal surface is relatively small. With an increase in velocity, the superior structural resistance of the cylinder surface over the flat surface gradually becomes apparent. In general, the ellipsoidal sub-floor reduces pressures at the side observably due to the bi-directional curvature.

Figure 15 illustrates the plastic strain nephogram at various time for different models when the velocity is 8 m/s. The distribution of plastic strain on the ellipsoid surface is more uniform, with severe plastic deformations not extensively concentrated. The ellipsoid under floor has a significant inward deflection on either side of the frame. It is able to better transfer the load from the skin to the frame, so the main energy absorbing components are utilised in an efficient manner.

The deformation of the skin during ditching is investigated. Considering that the mechanical properties of the aircraft floor frame are much better than the skin, it is worthwhile to set the frame as a rigid body to compare the changes in skin deflection. In addition, a longitudinal stiffener was installed at the longitudinal centreline of the new set of models, aiming to analyse the influence of longitudinal stiffeners on skin deflection during water impact. Figure 16 shows the vertical displacement contour map when the skin undergoes maximum deformation. When there is no longitudinal stiffener, the maximum deformation positions of the skin are all on the centreline. On this line, the midpoint is supported by the frame and no deformation occurs. The location of maximum deformation of the skin is not right in the middle of the two frames, but more towards the edge frames. The area of deformation of the flat

https://doi.org/10.1017/aer.2024.88 Published online by Cambridge University Press

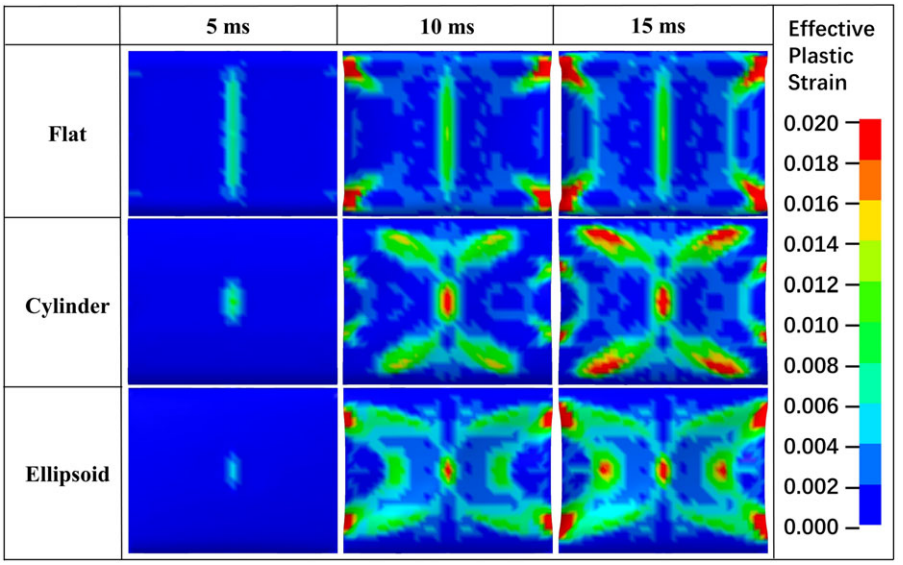


Figure 15. *Time histories of effective plastic strain at 8 m/s.*

floor is the largest, and the deflection value is also the largest, at 21.2 mm. The maximum deflection of the cylindrical floor is 18.3 mm. The deformation area of the ellipsoidal floor is the smallest, and the maximum deflection value is also the smallest, at 16.6 mm. After installing a longitudinal stiffener, the original maximum deformation positions are supported by the stiffener, and the deflection of all skins are greatly reduced, as shown in Fig. 17. The maximum deflection of the flat, elliptical and ellipsoidal floors decreases by 35.8%, 41.5% and 72.9%, respectively. The maximum deflection of the ellipsoidal floor with a longitudinal stiffener is only 4.5 mm. The results indicate that under water impact conditions, the longitudinal stiffener can significantly reduce skin deformation, and the elliptical floor has better mechanical performance than flat and cylindrical floors.

5. Conclusions and future works

A numerical simulation of the structures impact water is presented based on a coupled FE-SPH method. Numerical model validation is conducted with the experiment in the SPLASH project at the Laboratory for Impact Tests on Aerospace Structures. The peak acceleration and peak pressure at different locations on the under floor during water impact are investigated. The model is refined by adjusting contact parameters and particle density, resulting in simulation outcomes that closely align with experimental values.

Furthermore, the better shape of aircraft sub-floor structure is investigated in the case of ditching. This work proposes three types of aircraft sub-floor structures, including the flat under floor, the cylindrical under floor and the ellipsoidal under floor, designed to enhance impact resistance capacity to ensure skin integrity after water impact. The results show that the ellipsoidal under floor experiences lower peak acceleration during ditching compared to other shapes, effectively mitigating the impact forces on the structure. The curvature of the ellipsoidal surface diverts the water flow decreasing pressure loads at the sides. Additionally, the effect of the longitudinal stiffener on skin deflection during water impact was investigated. After the installation of longitudinal stiffeners, the deflection values of all skins decreased significantly. The maximum deflection of the ellipsoidal hull at 3 m/s is only 4.5 mm, much lower than the other shapes. And the plastic strain distribution on the ellipsoidal sub-floor is more uniform, improving

https://doi.org/10.1017/aer.2024.88 Published online by Cambridge University Press

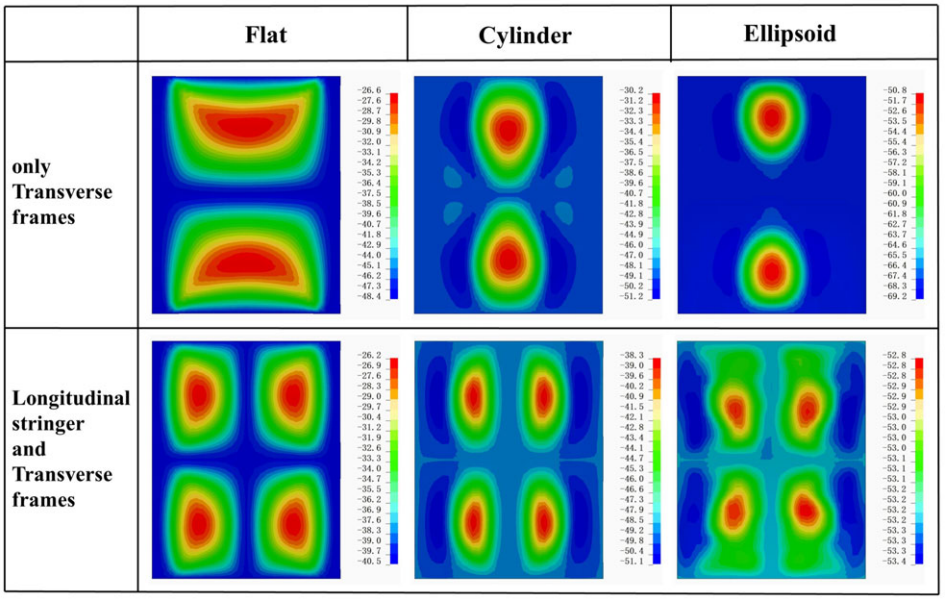


Figure 16. *The vertical displacement of the skin at 3 m/s.*

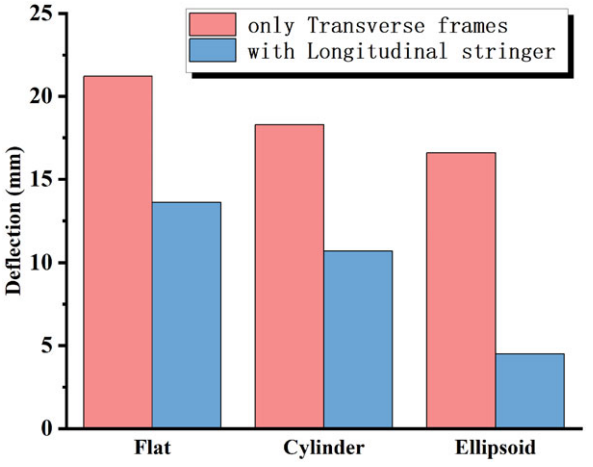


Figure 17. *Maximum deflection value of the skin at 3 m/s.*

resistance to rupture. Therefore, the ellipsoidal floor structure had better mechanical properties than the flat and cylindrical floor structures in the case of water impact.

In the roadmap of ditching for future development, a major challenge in predicting ditching loads is the inclusion of the effects of high velocity water flow on airframe loads, including effects such as cavitation, suction and aeration. To achieve the following objectives, it is necessary to investigate numerical methods and simulation, as well as experimental testing. Firstly, the methods should be demonstrated on representative aircrafts that use metallic, composite, and composite-metallic hybrid structures. Secondly, there is a significant difference in load between aircraft with horizontal speed and a helicopter during ditching. New experimental facilities need to be developed for in-water impact testing of structural components at horizontal velocities of 50–80 m/s to provide more realistic experimental data. Thirdly, to

https://doi.org/10.1017/aer.2024.88 Published online by Cambridge University Press

improve cavitation modelling, it is necessary to develop new models that consider the evolution of void fraction and the changing vapour and liquid during cavitation.

Acknowledgments. The present work is supported by the financial support from the National Natural Science Foundation of China (No. 52172356) and Hunan Provincial Natural Science Foundation of China (No. 2022JJ10012).

Supplementary material. To view supplementary material for this article, please visit https://doi.org/10.1017/aer.2024.88

References

[1] Hughes, K., Vignjevic, R., Campbell, J., De Vuyst, T., Djordjevic, N. and Papagiannis, L. From aerospace to offshore: Bridging the numerical simulation gaps–Simulation advancements for fluid structure interaction problems, *Int. J. Impact Eng.*, 2013, **61**, pp 48–63.
[2] Zheng, Y., Qu, Q., Liu, P., et al. Numerical analysis of the porpoising motion of a blended wing body aircraft during ditching, *Aerosp. Sci. Technol.*, 2021, **119**, p 107131.
[3] Von Karman, T.H. The impact on seaplane floats during landing (No. NACA-TN-321), 1929.
[4] Greenhow, M. Wedge entry into initially calm water. *Appl. Ocean Res.*, 1987, **9**, (4), pp 214–223.
[5] Faltinsen, O.M. Water entry of a wedge by hydroelastic orthotropic plate theory, *J. Ship Res.*, 1999, **43**, (03), pp 180–193.
[6] Seddon, C.M. and Moatamedi, M. Review of water entry with applications to aerospace structures, *Int. J. Impact Eng.*, 2006, **32**, (7), pp 1045–1067.
[7] Pentecôte, N. and Vigliotti, A. Crashworthiness of helicopters on water: Test and simulation of a full-scale WG30 impacting on water, *Int. J. Crashworthiness*, 2003, **8**, (6), pp 559–572.
[8] Yee, H.C., Sweby, P.K. and Griffiths, D.F. Dynamical approach study of spurious steady-state numerical solutions of non-linear differential equations. I. The dynamics of time discretization and its implications for algorithm development in computational fluid dynamics, *J. Comput. Phys.*, 1991, **97**, (2), pp 249–310.
[9] Hughes, K., Campbell, J. and Vignjevic, R. Application of the finite element method to predict the crashworthy response of a metallic helicopter under floor structure onto water, *Int. J. Impact Eng.*, 2008, **35**, (5), pp 347–362.
[10.] Hughes, K. and Campbell, J. Helicopter crashworthiness: A chronological review of research related to water impact from 1982 to 2006, *J. Am. Helicopter Soc.*, 2008, **53**, (4), pp 429–441.
[11] Fasanella, E.L., Boitnott, R.L., Lyle, K.H. and Jackson, K.E. Full-scale crash test and simulation of a composite helicopter, *Int. J. Crashworthiness*, 2001, **6**, (4), pp 485–498.
[12] Fasanella, E.L., Jackson, K.E., Sparks, C.E. and Sareen, A.K. Water impact test and simulation of a composite energy absorbing fuselage section, *J. Am. Helicopter Soc.*, 2005, **50**, (2), pp 150–164.
[13] Fasanella, E.L., Jackson, K.E. and Lyle, K.H. Finite element simulation of a full-scale crash test of a composite helicopter, *J. Am. Helicopter Soc.*, 2002, **47**, (3), pp 156–168.
[14] Dhileep, K., Kumar, D., Gautham Vigneswar, P.N., Soni, P., Ghosh, S., Ali, S.F. and Arockiarajan, A. Aerodynamic study of single corrugated variable-camber morphing aerofoil concept, *Aeronaut. J.*, 2022, **126**, (1296), pp 316–344.
[15] Rana, Z.A., Mauret, F., Sanchez-Gil, J.M., Zeng, K., Hou, Z., Dayyani, I. and Könözsy, L. Computational analysis and design of an aerofoil with morphing tail for improved aerodynamic performance in transonic regime, *Aeronaut. J.*, 2022, **126**, (1301), pp 1144–1167.
[16] Agarwal, D., Lu, L., Padfield, G.D., White, M.D. and Cameron, N. The use of augmented rotor inflow to predict rotorcraft responses in hover and low-speed manoeuvres, *Aeronaut. J.*, 2022, **126**, (1301), pp 1168–1186.
[17] Kumar, D., Singh, G., Mohite, P.M., Lau, E.M. and Wang, Y.-C. Role of flexibility on the aerodynamic performance of a resonating hummingbird-inspired wing, *Aeronaut. J.*, 2023, **127**, (1308): 193–212.
[18] Liu, M.B. and Liu, G. Smoothed particle hydrodynamics (SPH): an overview and recent developments, *Arch. Comput. Methods Eng.*, 2010, **17**, pp 25–76.
[19] Pérez, J.L., Benítez, L.H., Oliver, M. and Climent, H. Survey of aircraft structural dynamics non-linear problems and some recent solutions, *Aeronaut. J.*, 2011, **115**, (1173), pp 653–668.
[20] de Wit, A.J., van den Brink, W.M. and Moghadasi, M. Multiple unmanned aerial systems collision impacts on wing leading edge, *Aeronaut. J.*, 2022, **126**, (1304), pp 1648–1677.
[21] CAST Crashworthiness of Helicopters on Water: Design of Structures Using Advanced Simulation Tools, Project G4RD-CT-2000-00178 partially funded by the European Union under the Aeronautics part of the FP5-GROWTH RTD, 2000–2003. https://cordis.europa.eu/project/rcn/52827_en.html (accessed October 2018).
[22] D. Delsart, GARTEUR HC/AG-15: improvement of SPH methods for application to helicopter ditching, 2007–2010, http://www.garteur.org/Action (accessed October 2018).
[23] Francesconi, E. and Anghileri, M. Towards a methodology to design water impact crashworthy structures, In *66th American Helicopter Society International Annual Forum 2010*, 2010 (pp. 222–233). Curran Associates.
[24] Toso-Pentecôte, N., Delsart, D., Vagnot, A. and Kindervater, C. Evaluation of Smooth Particle Hydrodynamic methods for the simulation of helicopter ditching, 2010.
[25] Smart Aircraft in Emergency Situations, Project 266172 partially funded by the European Union under FP7-TRANSPORT, 2011–2014, https://cordis.europa.eu/project/rcn/97150_en.html (accessed October 2018).
[26] Woodgate, M.A. and Barakos, G.N. Implicit computational fluid dynamics methods for fast analysis of rotor flows, *AIAA J.*, 2012, **50**, (6), pp 1217–1244.

https://doi.org/10.1017/aer.2024.88 Published online by Cambridge University Press

[27] Xiao, T., Qin, N., Lu, Z., Sun, X., Tong, M. and Wang, Z. Development of a smoothed particle hydrodynamics method and its application to aircraft ditching simulations, *Aerosp. Sci. Technol.*, 2017, **66**, pp 28–43.
[28] Woodgate, M.A., Barakos, G.N., Scrase, N. and Neville, T. Simulation of helicopter ditching using smoothed particle hydrodynamics, *Aerosp. Sci. Technol.*, 2019, **85**, pp 277–292.
[29] Lucy, L.B. A numerical approach to the testing of the fission hypothesis, *Astronom. J.*, 1977, **82**, pp 1013–1024.
[30] Gingold, R.A. and Monaghan, J.J. Smoothed particle hydrodynamics: theory and application to non-spherical stars, *Mon. Not. R. Astron. Soc.*, 1977, **181**, (3), pp 375–389.
[31] Authority, C.A. *Summary Report on Helicopter Ditching and Crashworthiness Research*. The Stationary Office, Norwich, UK, 2005.
[32] Vignjevic, R. and Meo, M. A new concept for a helicopter sub-floor structure crashworthy in impacts on water and rigid surfaces, *Int. J. Crashworthiness*, 2002, **7**, (3), pp 321–330.
[33] Ren, Y. and Xiang, J. Crashworthiness uncertainty analysis of typical civil aircraft based on Box–Behnken method, *Chin. J. Aeronaut.*, 2014, **27**, (3), pp 550–557.
[34] Taber, M.J. Crash attenuating seats: Effects on helicopter underwater escape performance, *Saf. Sci.*, 2013, **57**, pp 179–186.
[35] Ren, Y. and Xiang, J. The crashworthiness of civil aircraft using different quadrangular tubes as cabin-floor struts, *Int. J. Crashworthiness*, 2011, **16**, (3), pp 253–262.
[36] Thuis, H.C.S.J. and Wiggenraad, J.F.M. A tensor-skin concept for crashworthiness of helicopters in case of water impact, In *Annual Forum Proceedings-American Helicopter Society* (Vol. 5, pp. 547–547). American Helicopter Society, 1994.
[37] Brooks, C.J., MacDonald, C.V., Donati, L. and Taber, M.J. Civilian helicopter accidents into water: Analysis of 46 cases, 1979–2006, *Aviat. Space Environ. Med.*, 2008, **79**, (10), pp 935–940.
[38] De Florio, F. *Airworthiness: An Introduction to Aircraft Certification and Operations*. Butterworth-Heinemann, 2016.
[39] Borrelli, R., Ignarra, M. and Mercurio, U. Experimental investigation on the water impact behavior of composite structures, *Proc. Eng.*, 2014, **88**, pp 85–92.
[40] Toso, N.R.S. Contribution to the modelling and simulation of aircraft structures impacting on water, 2009.
[41] Borrelli, R., Mercurio, U. and Alguadich, S. Water impact tests and simulations of a steel structure, *Int. J. Struct. Integr.*, 2012, **3**, (1), pp 5–21.
[42] Grimaldi, A., Benson, D.J., Marulo, F. and Guida, M. Steel structure impacting onto water: Coupled finite element-smoothed-particle-hydrodynamics numerical modeling, *J. Aircr.*, 2011, **48**, (4), pp 1299–1308.
[43] Cobb, B.R., Tyson, A.M. and Rowson, S. Head acceleration measurement techniques: reliability of angular rate sensor data in helmeted impact testing, *Proc. Inst. Mech. Eng. P: J. Sports Eng. Technol.*, 2018, **232**, (2), pp 176–181.

Cite this article: Wang B., Nie L. and Ren Y. (2024). Numerical simulation of different aircraft sub-floor structures during ditching. *The Aeronautical Journal*, **128**, 2530–2544. https://doi.org/10.1017/aer.2024.88

https://doi.org/10.1017/aer.2024.88 Published online by Cambridge University Press